Connectome Smoothing and a Law of Large Graphs

Runze Tang[1], Michael Ketcha[2], Joshua T. Vogelstein[2],
Carey E. Priebe[1], Daniel L. Sussman[3*]

1 Department of Applied Math & Statistics, The Johns Hopkins University, Baltimore, MD
2 Department of Biomedical Engineering, The Johns Hopkins University, Baltimore, MD
3 Department of Mathematics & Statistics, Boston University, Boston, MA
* sussman@bu.edu

Abstract

Estimating the mean of a population of graphs based on a sample is a core problem in network science. Often, this problem is especially difficult because the sample or cohort size is relatively small as compared to the number of parameters to estimate. While using the element-wise sample mean of the adjacency matrices is a common approach, this method does not exploit any underlying graph structure. We propose using a low-rank method together with tools for dimension selection and diagonal augmentation to improve performance over the naive methodology for small sample sizes. Theoretical results for the stochastic blockmodel show that this method will offer major improvements when there are many vertices. Similarly, in analyzing human connectome data, we demonstrate that the low-rank methods outperform the standard sample mean for many settings. These results indicate that low-rank methods should be an important part of the tool box for researchers studying populations of graphs.
Keywords: networks, connectome, low-rank, estimation

1 Introduction

Estimation of the mean of a population based on samples is at the core of statistics. The sample mean, motivated by the law of large numbers and the central limit theorem, has its place as one of the most important statistics for this task. In modern settings, we take averages almost everywhere, from data in Euclidean space to more complex objects like shapes, documents, and graphs.

The mean of a population of graphs is a high dimensional object, consisting of $O(N^2)$ parameters for a graph with N vertices. Estimating high dimensional estimands with a small sample size using naive unbiased methods often leads to inaccurate estimates with very high variance. By exploiting a bias-variance trade-off, it is often fruitful to develop estimators which have some

1

bias but greatly reduced variance. When these estimators are biased towards low-dimensional structures which well approximate the full dimensional population mean, major improvements can be realized [Trunk, 1979].

In statistical decision theory, we say that a procedure δ' improves another procedure δ if and only if the risk of δ' is no bigger than the risk of δ all the time, and strictly less than the risk of δ for in some situations. If there exists a decision procedure δ' which improves δ, then δ is said to be inadmissible. So generally, inadmissible procedure is not preferred since there is another choice which is always "better" than it. However, in a striking result, Stein [1956] and James and Stein [1961] showed the arithmetic average should not always be the first choice and is inadmissible in even simple settings by today's standards. In particular, James and Stein showed that the sample mean for a multivariate normal distribution with at least three dimensions is inadmissible and can be strictly improved by carefully biasing the estimate towards any given fixed point. Twenty-seven years later, Gutmann [1982] proved that this phenomenon cannot occur when the sample spaces are finite. But even when the sample mean is admissible, this doesn't mean that other estimators should not be used in all cases. In many situations where other structural information is hypothesized, for instance a collection of graphs as considered in this paper, other estimators may be preferable.

In complex data settings such as shape data, language data, or graph data, we also must take care in how we define the mean. As with real valued data, one may want to define the mean of a population of graphs to be a graph such as for the median graph [Jiang et al., 2001]. However, this may be too restrictive for populations of graphs where there is high variation in which edges appear. Instead, for a collection of graphs sampled from a larger population, we define the mean graph as the weighted adjacency matrix with weights given by the proportion of times the corresponding edge appears in the population. As we will describe below, this definition of the mean graph is the expectation of the adjacency matrix. This population mean is becoming more and more important both in statistical inference and in various applications like connectomics, social networks, and computational biology.

Ginestet et al. [2014] proposed a way to test if there is a difference between the distributions for two groups of networks. While hypothesis testing is the end goal of their work, estimation is a key intermediate step which may be improved by accounting for underlying structure in the mean matrix. Thus, improving the estimation procedures for the mean graph is not only important by itself, but also can be applied to help improve other statistical inference procedures.

To better illustrate the idea, we take the CoRR brain graphs with Desikan atlases as an example. The dataset contains 454 brain scans with 70 vertices. Each vertex represents a region defined by the Desikan atlases, while an edge exists between two vertices if there is at least one white-matter tract connecting the corresponding regions of the brain. More details are given in Section 4.3 and Section 6.3. By observing M graphs sampled from the 454 graphs, our goal is to estimate the mean graph of the population P, defined as the entry-wise mean of all the 454 graphs. We plot the population mean graph P on the left

2

panel in Fig. 1.

The element-wise sample mean is a reasonable estimator if we consider the general independent edge model (IEM) [Bollobás et al., 2007] without taking any additional structure into account. However, with only a small sample size, such as when the sample size is much less than the number of vertices, it does not perform very well. Now take a sample of size $M = 5$ in the CoRR dataset example, we calculate the entry-wise sample mean $\bar{A}$ and plot in the center of Fig. 1. We can see $\bar{A}$ gives a fair estimate of P. However, since the sample size is small, there are a lot of pairs of vertices with no edges or 5 edges in the 5 observations. This leads to the white and black pixels in the image corresponding to $\bar{A}$. On the other hand, $\widehat{P}$ has a finer gradient of values which in this case leads to a more accurate estimate. Intuitively, an estimator incorporating structure in the distribution of graphs, assuming the estimator is computationally tractable, is preferable to the entry-wise sample mean. In general, we don't have any knowledge about this structure so it can be hard to take advantage of in practice.

One of the most important structures in graphs is the community structure in which vertices are clustered into groups that share similar connectivity structure. The stochastic blockmodel (SBM) [Holland et al., 1983] is one model that captures this structural property and is widely used in modeling networks. From population mean P plotted in Fig. 1, we can see the brain is a 2-block model at the highest level, representing the two hemispheres. More generally, the latent positions model (LPM) [Hoff et al., 2002], provides a way to parameterize the graph structure by latent positions associated with each vertex. Latent position models can capture strong community structure like the stochastic blockmodel, but may also allow for more variance within communities and other structures. One example of an LPM which captures this middle ground is the random dot product graph (RDPG) [Young and Scheinerman, 2007, Nickel, 2007] which motivates our estimator. It generalizes the positive semi-definite SBM by allowing for mixed membership and degree corrections.

Using estimates of the latent positions based on a truncated eigen-decomposition of the adjacency matrix, we propose an estimator which captures the low-rank structure of the mean graph for the RDPG model. These estimates will improve performance since they will be biased towards the low-rank structure of the RDPG model and will have much lower overall variance than naive element-wise sample means. Here we consider the same random sample of size $M = 5$ based on the Desikan atlas in Fig. 1 and plot the estimate $\widehat{P}$ in the right panel. Note that compared to the sample mean $\bar{A}$, $\widehat{P}$ has a finer gradient of values which in this case leads to a more accurate estimate of the true probability matrix P, especially for edges between the two hemispheres, in the upper right and corresponding lower left block. In this study, we show via theory, simulations, and real data analysis that the low-rank estimator frequently outperforms the element-wise sample mean, especially in small sample sizes.

In Section 2, we outline a nested collection of models which we consider for our theorems and simulations, and in Section 3 we describe the entry-wise sample mean and introduce our specific low-rank estimator, which accounts
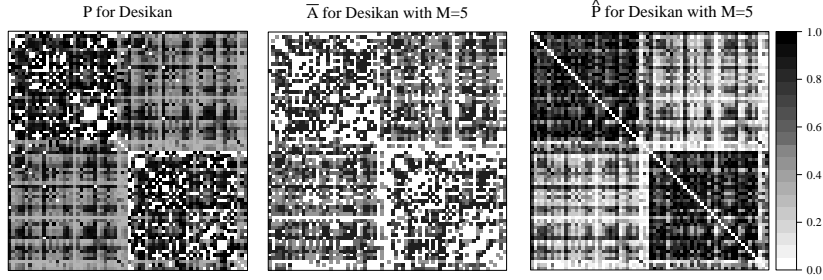
3

Fig 1: **Heat maps of the population mean, the sample mean, and the estimator $\widehat{P}$.** These heat maps indicate the population mean for the 454 graphs (left), sample mean for the 5 sampled graphs (center), and $\widehat{P}$ for the 5 sampled graphs with dimension $d = 11$ selected using the Zhu and Ghodsi method (right). Darker pixels indicate a higher probability of an edge between the given vertices. Note that $\widehat{P}$ appears to better estimate the true probability matrix P, especially for edges between the two hemispheres, in the upper right and corresponding lower left block.

for the unknown dimension and attempts to correct for other issues found in real world problems. Our main results are presented in Section 4 where we present theorems and simulations for the stochastic blockmodel, an investigation of a connectome dataset, and a synthetic data analysis. We conclude with a discussion of these results in Section 5 and with details on our proposed method and the data which is analyzed in Section 6.

2 Models

This work considers the scenario of having M graphs, represented as adjacency matrices, $\{A^{(m)}\}$ $(m = 1, \cdots, M)$, each having N vertices with $A^{(m)} \in \{0, 1\}^{N \times N}$. We assume there is a known correspondence for vertices in different graphs, so that vertex i in graph m corresponds to vertex i in graph m' for any i, m, m'. The graphs we consider are undirected and unweighted with no self-loops, so each $A^{(m)}$ is a binary symmetric matrix with zeros along the diagonal. An example application of this arises in the field of connectomics, where brain imaging data for each subject can be represented as a graph, where each vertex represents a well-defined anatomical region present in each subject. For structural brain imaging, an edge may represent the presence of anatomical connections between the two regions as estimated based on tractography for diffusion tensor magnetic resonance imaging. Similarly, for functional data, an edge between two regions may represent the presence of correlated brain activity between the two regions.

For the purpose of this paper, we also assume that the graphs are sampled independently and identically from some distribution. To this end, the mean

4

graph is the expectation of each adjacency matrix.

Definition 2.1 (Mean Graph)**.** *Suppose that* $A^{(1)}, \ldots, A^{(M)} \overset{iid}{\sim} \mathcal{G}$ *for some random graph distribution* $\mathcal{G}$, *with* $A^{(m)} \in \{0,1\}^{N \times N}$ *for each* m. *The* mean graph *is defined as* $\mathbb{E}[A^{(m)}]$, *where since the graphs are identically distributed* $\mathbb{E}[A^{(m)}] = \mathbb{E}[A^{(m')}]$ *for any* m, m'.

We present here three nested models for these distributions, the independent edge model, the random dot product model, and the (positive semi-definite) stochastic blockmodel. In Section 3, we present two estimators motivated by these models.

2.1 Independent Edge Model

The first model we consider is the independent edge model (IEM) with parameter $P \in [0,1]^{N \times N}$ [Bollobás et al., 2007]. An edge exists between vertex i and vertex j with probability P_{ij} and each edge is present independently of all other edges. For this case, we aim to estimate the mean graph $P = \mathbb{E}[A^{(m)}]$ based on the observed adjacency matrices $A^{(1)}, \ldots, A^{(M)}$.

2.2 Random Dot Product Graph

In graphs, the adjacencies between vertices generally depend on unobserved properties of the corresponding vertices. For example, in a connectomics setting, the two brain regions with similar properties will have similar connectivity patterns to other regions of the brain. The latent positions model (LPM) proposed by Hoff et. al. (2002) [Hoff et al., 2002] captures such structure, where each vertex is associated with a latent position that influences the adjacencies for that vertex. In this model, each vertex i has an associated latent vector $X_i \in \mathbb{R}^d$. Conditioned on the latent positions, the existence of each edge is independent and the probability the edge is present only depends on the latent vectors of the incident vertices through a link function. If d is much smaller than the number of vertices N and the link function is known, LPMs are more parsimonious models compared to IEM, requiring only dN parameters rather than $\binom{N}{2}$.

A specific instance of an LPM that we examine in this work is the random dot product graph model (RDPG) [Young and Scheinerman, 2007, Nickel, 2007] where the link function is the dot product, so the probability of an edge being present between two nodes is the dot product of their latent vectors. The direction of the latent position is determined by properties of that vertex, and vertices whose latent positions point in similar directions are more likely to have an edge between them than vertices whose latent positions point in orthogonal directions. Similarly, the magnitudes of the latent position encode the vertices' overall tendency to form edges, with a larger magnitude leading to more edges incident with the vertex.

Formally, let $\mathcal{X} \subset \mathbb{R}^d$ be a set such that $x, y \in \mathcal{X}$ implies $\langle x, y \rangle = \sum_i x_i y_i \in [0,1]$. Let $X_1, \ldots, X_n \in \mathcal{X}$ and write $X = [X_1 | \cdots | X_N]^\top \in \mathbb{R}^{N \times d}$. A random

graph G with adjacency matrix A is said to be an RDPG if

$$\Pr[A|X] = \prod_{i<j} \langle X_i, X_j \rangle^{A_{ij}} \left(1 - \langle X_i, X_j \rangle\right)^{1-A_{ij}}.$$

In the RDPG model, each vertex i is associated with latent position X_i, and conditioned on the latent positions X, the entries A_{ij} are distributed independently as Bernoulli($\langle X_i, X_j \rangle$) for $i < j$. Note that the probability matrix is the outer product of the latent position matrix with itself, $P = XX^\top$. This imposes two properties on P, namely that P is positive-semidefinite and $\operatorname{rank}(P) = \operatorname{rank}(X) \leq d$. These properties lead us to our proposed estimator.

2.3 Stochastic Blockmodel as a Random Dot Product Graph

One of the most important structures for graphs is the community structure in which vertices are clustered into different communities such that vertices of the same community behave similarly. This structural property is captured by the stochastic blockmodel (SBM) [Holland et al., 1983], where each vertex is assigned to a block and the probability that an edge exists between two vertices depends only on their respective block memberships.

Reviewer 3 mentioned the following references. Ambroise and Matias [2012], Wolfe and Olhede [2013], Choi et al. [2012], Picard et al. [2009], Zanghi et al. [2008, 2010], Pavlovic et al. [2014], Daudin et al. [2008].

The SBM is parameterized by the number of blocks K (generally much less than the number of vertices N), the block probability matrix $B \in [0,1]^{K \times K}$, and the vector of block memberships $\tau \in \{1, \ldots, K\}^N$, where for each $i \in [N]$, $\tau_i = k$ means vertex i is a member of block k.

Conditioned on τ, each entry of the adjacency matrix A_{ij} is independently sampled from the Bernoulli distribution with parameter B_{τ_i, τ_j}. To ensure that the SBM can be considered as an RDPG, we impose that the B matrix for the SBM is positive semidefinite. For notational convenience we will refer to the sub-model of the SBM with positive semidefinite B matrix as the SBM.

In order to analyze the estimator $\widehat{P}$ motivated by RDPG, we will represent the SBM as an RDPG by decomposing B as $\nu \nu^\top$, where $\nu \in \mathbb{R}^{K \times d}$ and each row ν_k is the shared latent position for all vertices assigned to block k. For $X \in \mathbb{R}^{N \times d}$ with rows given by $X_i = \nu_{\tau_i}$, we have

$$\Pr[A_{ij} = 1 | \tau] = B_{\tau_i, \tau_j} = \nu_{\tau_i}^\top \nu_{\tau_j}.$$

In this way, the SBM can be seen as an RDPG where all vertices in the same block will have identical latent positions.

An example SBM is illustrated in Fig. 2. We consider a 5-block SBM and plot the corresponding probability matrix and one adjacency matrix generated from it with 200 vertices. From the top two panels of the figure, we can clearly see the structure of 25 blocks in both the probability matrix and the adjacency matrix as a result of 5 different blocks among vertices.

6

3 Estimators

In this section, we present two estimators, the standard element-wise sample mean $\bar{A}$, and a low-rank estimator $\widehat{P}$. We describe the low-rank aspects of this estimator in this section and present further important details regarding diagonal augmentation and dimension estimation in Section 6.

3.1 Element-wise sample mean $\bar{A}$

The most natural estimator to consider is to take the average of the observed adjacency matrices which yields the element-wise sample mean. This estimator, defined as $\bar{A} = \frac{1}{M} \sum_{m=1}^{M} A^{(m)}$, is the maximum likelihood estimator (MLE) for the mean graph P if the graphs are sampled from an IEM distribution. It is unbiased so $\mathbb{E}[\bar{A}] = P$ with entry-wise variance $\text{Var}(\bar{A}_{ij}) = P_{ij}(1 - P_{ij})/M$. Moreover, $\bar{A}$ is the uniformly minimum-variance unbiased estimator, so it has the smallest variance among all unbiased estimators and enjoys the many asymptotic properties of the MLE as $M \to \infty$ for fixed N. However, if graphs with a large number of vertices are of interest, there are no useful asymptotic properties for $\bar{A}$ as the number of vertices N becomes large for fixed M.

Additionally, $\bar{A}$ doesn't exploit any graph structure. If the graphs are distributed according to an RDPG or SBM, then $\bar{A}$ is no longer the maximum likelihood estimator since it is not guaranteed to satisfy the properties of the mean graph for that model. The performance can be especially poor when the sample size M is small, such as when $M \ll N$. For example, when $M = 1$, $\bar{A}$ is simply the binary adjacency matrix $A^{(1)}$, which is an inaccurate estimate for an arbitrary P compared to estimates which exploit underlying structure, such as occurs for the RDPG.

3.2 Low-Rank Estimator $\widehat{P}$

Motivated by the low-rank structure of the RDPG mean matrix, we propose the estimator $\widehat{P}$ based on the spectral decomposition of $\bar{A}$ which yields a low rank approximation of $\bar{A}$. This estimator is similar to the estimator proposed by Chatterjee [2015] but additionally we propose adjustments to canonical low-rank methods which serve to improve the performance for the specific task of estimating the mean graph. Additionally, we consider an alternative dimension selection technique as discussed in Section 6.1.

For a given dimension d we consider the estimator $\text{lowrank}_d(\bar{A})$ defined as the best rank-d positive-semidefinite approximation of $\bar{A}$. Since the graphs are symmetric, we can compute the eigen-decomposition of $\bar{A}$ as $\widehat{U}\widehat{S}\widehat{U}^{\top} + \tilde{U}\tilde{S}\tilde{U}^{\top}$, where $\widehat{S}$ is a diagonal matrix with non-increasing entries along the diagonal corresponding to the largest d eigenvalues of $\bar{A}$, and $\widehat{U}$ has columns given by the corresponding eigenvectors. Similarly, $\tilde{S}$ is the diagonal matrix with non-increasing entries along the diagonal corresponding to the rest $N-d$ eigenvalues of $\bar{A}$, and $\tilde{U}$ has the columns given by the corresponding eigenvectors. The d-dimensional adjacency spectral embedding (ASE) of $\bar{A}$ is given by $\widehat{X} = \widehat{U}\widehat{S}^{1/2} \in$
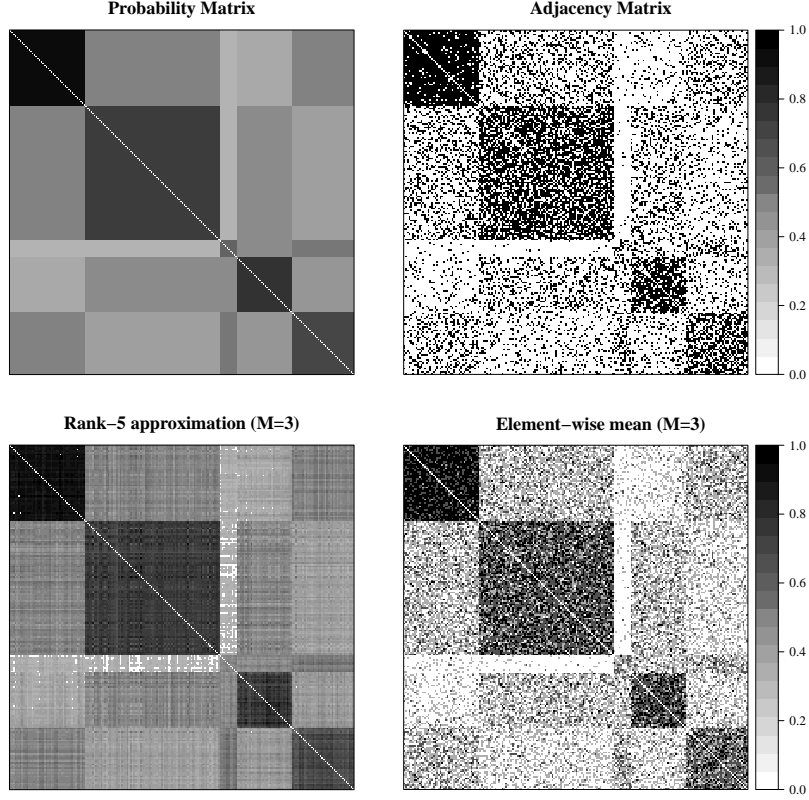
7

Fig 2: Example illustrating the stochastic blockmodel. The top left figure shows the mean graph P with $K = 5$ blocks and $N = 200$ vertices and the top right figure shows an adjacency matrix A sampled according to the probabilities from P. While A is a noisy version of P, much of the structure of P is preserved in A, a property we will exploit in our estimation procedure. Based on three graphs sampled independently and identically according to the probability matrix P, we construct the element-wise mean $\bar{A}$, shown in the lower right panel (see Section 3.1). Finally, by taking a rank-5 approximation of $\bar{A}$ and thresholding the values to be between 0 and 1, we construct our proposed estimate $\widehat{P}$, shown in the lower left panel (see Section 3.2). By visual inspection, it is clear that the low-rank estimate $\widehat{P}$ more closely approximates the probability matrix P as compared to $\bar{A}$.

$\mathbb{R}^{N \times d}$. For an RDPG, the rows of $\widehat{X}$ are estimates of the latent vectors for each vertex [Sussman et al., 2014]. Using the adjacency spectral embedding, we have that the low-rank approximation of $\bar{A}$ is $\widehat{X}\widehat{X}^\top = \widehat{U}\widehat{S}\widehat{U}^\top$. Algorithm 1 gives the steps to compute this low-rank approximation.

Algorithm 1 Algorithm to compute the rank-d approximation of a matrix.

Input: Symmetric matrix $A \in \mathbb{R}^{N \times N}$ and dimension $d \leq N$.
Output: lowrank$_d(A) \in \mathbb{R}^{N \times N}$
 1: Compute the algebraically largest d eigenvalues of A, $s_1 \geq s_2 \geq \ldots \geq s_d$ and corresponding unit-norm eigenvectors $u_1, u_2, \ldots, u_d \in \mathbb{R}^N$;
 2: Set $\widehat{S}$ to the $d \times d$ diagonal matrix diag$(s_1, \ldots, s_d)$;
 3: Set $\widehat{U} = [u_1, \ldots, u_d] \in \mathbb{R}^{N \times d}$;
 4: Set lowrank$_d(A)$ to $\widehat{U}\widehat{S}\widehat{U}^\top$;

To compute our estimator $\widehat{P}$, we also need to specify what rank d to use and there are various ways of dealing with dimension selection. In this paper, we use an elbow selection method proposed in Zhu and Ghodsi [2006] and the universal singular value thresholding (USVT) method [Chatterjee, 2015]. Details for these methods are discussed in Section 6.1.

Moreover, since the adjacency matrices are hollow, with zeros along the diagonal, there is a missing data problem that leads to inaccuracies if we compute $\widehat{P}$ based only on $\bar{A}$. To compensate for this issue, we use an iterative method developed in Scheinerman and Tucker [2010]. Details are discussed in Section 6.2.

Algorithm 2 Algorithm to compute $\widehat{P}$

Input: Adjacency matrices $A^{(1)}, A^{(2)}, \cdots, A^{(M)}$, with each $A^{(m)} \in \{0,1\}^{N \times N}$
Output: Estimate $\widehat{P} \in [0,1]^{N \times N}$

 1: Calculate the sample mean $\bar{A} = \frac{1}{M} \sum\limits_{m=1}^{M} A^{(m)}$;
 2: Calculate the scaled degree matrix $D^{(0)} = \text{diag}(\bar{A}\mathbf{1})/(N-1)$;
 3: Select the dimension d based on the eigenvalues of $\bar{A}+D^{(0)}$; (see Section 6.1)

 4: Set $\tilde{P}^{(0)}$ to lowrank$_d(\bar{A} + D^{(0)})$; (see Algorithm 1)
 5: Set $D^{(1)}$ to diag$(\tilde{P}^{(0)})$, the diagonal matrix with diagonal matching $\tilde{P}^{(0)}$;
 6: Set $\tilde{P}^{(1)}$ to lowrank$_d(\bar{A} + D^{(1)})$; (see Algorithm 1)
 7: Set $\widehat{P}$ to $\tilde{P}^{(1)}$ with values < 0 set to 0 and values > 1 set to 1.

Algorithm 2 gives the steps involved to compute the low-rank estimate $\widehat{P}$. As we will see in the succeeding sections, this procedure will frequently yield improvements in estimation as compared to using the sample mean $\bar{A}$. While this is unsurprising for random dot product graphs, where we are able to show theoretical results to this effect, we also see this effect for connectome data and more general independent edge graphs. In the following sections, we explore

this estimator in the context of the stochastic blockmodel.

The bottom panels of Fig. 2 demonstrate the two estimators $\widehat{P}$ and $\bar{A}$ for the stochastic blockmodel given by the upper left panel. The estimates are based on a sample of size $M = 3$ and in this instance visual inspection demonstrates that $\widehat{P}$ performs much better than $\bar{A}$.

4   Results

4.1   Asymptotic Theory

To estimate the mean of a collection of graphs, we consider the two estimators from Section 3: the entry-wise sample mean $\bar{A}$ and the low-rank $\widehat{P}$ motivated by the RDPG. We evaluate our estimators in terms of mean squared error, either $\mathrm{MSE}(\widehat{P}_{ij}) = \mathbb{E}[\widehat{P}_{ij} - P]^2$ or $\mathrm{MSE}(\bar{A}) = \mathbb{E}[\bar{A}_{ij} - P]^2$. While we can directly compare the difference in mean squared errors between the two estimators, it is frequently useful to consider the relative efficiency between two estimators. In our case, this is $\mathrm{RE}(\bar{A}_{ij}, \widehat{P}_{ij}) = \frac{\mathrm{MSE}(\widehat{P}_{ij})}{\mathrm{MSE}(\bar{A}_{ij})}$, with values above 1 indicating $\bar{A}$ should be preferred while values below 1 indicate $\widehat{P}$ should be preferred. Relative efficiency is a useful metric for comparing estimators because it will frequently be invariant to the scale of the noise in the problem and hence is more easily comparable across different settings.

In this section, we analyze the performance of these two estimators under the SBM by computing the entry-wise relative efficiency (RE). We also consider the asymptotic relative efficiency, which is the limit of the relative efficiency as the number of vertices $N \to \infty$ but with the number of graphs M fixed, and the scaled relative efficiency, $N \cdot \mathrm{RE}(\bar{A}_{ij}, \widehat{P}_{ij})$ which in our case normalizes the relative efficiency so that the asymptotic scaled relative efficiency is non-zero and finite. Somewhat surprisingly, we will see that the asymptotic relative efficiency will not depend on this fixed sample size M.

For this asymptotic framework, we assume the block memberships τ_i are drawn iid from a categorical distribution with block membership probabilities given by $\rho \in [0, 1]^K$. In particular, this implies that for each block k, the proportion $|\{i : \tau_i = k\}|/N$ of vertices in block k will converge to ρ_k as $N \to \infty$. We will also assume that for a given N, the block membership probabilities are fixed for all graphs. Denote block probability matrix $B = \nu\nu^\top$. By definition, the mean of the collection of graphs generated from this SBM is P, where $P_{ij} = B_{\tau_i, \tau_j}$. After observing M graphs on N vertices $A^{(1)}, \cdots, A^{(M)}$ sampled independently from the SBM conditioned on τ, we can calculate the two estimators $\bar{A}$ and $\widehat{P}$.

Lemma 4.1. *For the above setting, for any i, j, if $\mathrm{rank}(B) = K = d$, we have*

$$\lim_{N \to \infty} N \cdot \mathrm{Var}(\widehat{P}_{ij}) = \frac{1/\rho_{\tau_i} + 1/\rho_{\tau_j}}{M} P_{ij}(1 - P_{ij}),$$

and for large enough N, we have

$$\mathbb{E}[(\widehat{P}_{ij} - P_{ij})^2] \approx \frac{1/\rho_{\tau_i} + 1/\rho_{\tau_j}}{MN} P_{ij}(1 - P_{ij}).$$

The first part of this Lemma gives the form of the asymptotic variance of $\widehat{P}$ and the second part ensures that the estimator is asymptotically unbiased for P. The proof of this lemma is outlined in Section 6.4 and is based on results for the variance of the adjacency spectral embedding from Athreya et al. [2013]. From the result, we can see that the MSE of $\widehat{P}_{ij}$ is of order $O(M^{-1}N^{-1})$ approximately. Similar to $\bar{A}$, the estimate will get better as the number of observations M increases. Furthermore, it also benefits from a larger graph because of the use of low-rank structure. That is, $\widehat{P}$ will perform better as the number of vertices of the graph N increases.

Moreover, since $\bar{A}_{ij}$ is the sample mean of M independent Bernoulli random variables with parameter P_{ij}, we have

$$\mathbb{E}[(\bar{A}_{ij} - P_{ij})^2] = \frac{P_{ij}(1 - P_{ij})}{M}.$$

Based on this MSE result of $\bar{A}_{ij}$ and the MSE result of $\widehat{P}_{ij}$ given by Lemma 4.1, we can conclude the following theorem naturally.

Theorem 4.2. *In the same setting as in Lemma 4.1, for any i and j, if* $\mathrm{rank}(B) = K = d$, *then for large enough N, we have*

$$\mathrm{RE}(\bar{A}_{ij}, \widehat{P}_{ij}) \approx \frac{1/\rho_{\tau_i} + 1/\rho_{\tau_j}}{N}. \tag{1}$$

And the asymptotic relative efficiency (ARE) is

$$\mathrm{ARE}(\bar{A}_{ij}, \widehat{P}_{ij}) = \lim_{N \to \infty} \mathrm{RE}(\bar{A}_{ij}, \widehat{P}_{ij}) = 0.$$

Proof. Combine the MSE result of $\bar{A}_{ij}$

$$\mathbb{E}[(\bar{A}_{ij} - P_{ij})^2] = \frac{P_{ij}(1 - P_{ij})}{M},$$

and Lemma 4.1, i.e. for large enough N,

$$\mathbb{E}[(\widehat{P}_{ij} - P_{ij})^2] \approx \frac{1/\rho_{\tau_i} + 1/\rho_{\tau_j}}{MN} P_{ij}(1 - P_{ij}),$$

we have for large enough N,

$$\mathrm{RE}(\bar{A}_{ij}, \widehat{P}_{ij}) = \frac{\mathrm{MSE}(\widehat{P}_{ij})}{\mathrm{MSE}(\bar{A}_{ij})} = \frac{\mathbb{E}[(\widehat{P}_{ij} - P_{ij})^2]}{\mathbb{E}[(\bar{A}_{ij} - P_{ij})^2]} \approx \frac{1/\rho_{\tau_i} + 1/\rho_{\tau_j}}{N}.$$

And the ARE result follows directly by taking the limit of RE as $N \to \infty$. $\quad\square$

This theorem indicates that under the SBM, $\widehat{P}$ is a much better estimate of the mean of the collection of graphs P than $\bar{A}$. Note that a relative efficiency less than 1 indicates that $\widehat{P}$ should be preferred over $\bar{A}$, so under the above assumptions, as $N \to \infty$, $\widehat{P}$ performs far better than $\bar{A}$. From the result, we see that the relative efficiency is of order $O(N^{-1})$ and $N \cdot \mathrm{RE}(\bar{A}_{ij}, \widehat{P}_{ij})$ converges to $1/\rho_{\tau_i} + 1/\rho_{\tau_j}$ when $N \to \infty$. An important aspect of Theorem 4.2 is that the ARE does not depend on the number of graphs M, so the larger the graphs are, the better $\widehat{P}$ is relative to $\bar{A}$, regardless of M.

Note that the asymptotic result here is for number of vertices going to infinity with a fixed number of graphs. Such setting is very useful in connectomics analysis since we anticipate the collection of larger and larger brain network which will also likely initially correspond to smaller sample sizes as the technology to scale these connectome collection techniques is developed.

The approximate formula Eq. 1 indicates that the sizes of the blocks can greatly impact the relative efficiency. As an example, consider a two block stochastic model. If each of the blocks contain half the vertices, then for each pair of vertices, the relative efficiency is approximately $4/N$. If the first block gets larger, with $\rho_1 \to 1$, then the RE for estimating P_{ij} with $\tau_i = \tau_j = 1$ will tend to its minimum of $2/N$. On the other hand as $\rho_1 \to 1$, if $\tau_i = 1$ and $\tau_j = 2$, then since $\rho_2 = 1 - \rho_1$, the relative efficiency for estimating such an edge pair will be approximately 1 and the same will hold if $\tau_i = \tau_j = 2$. Note that the maximum value for the relative efficiency in a two-block model is achieved when $\rho_1 = 1/N$ and $\rho_2 = (N-1)/N$ in which case the relative efficiency is $N/(N-1) \approx 1$. (Note values of ρ_s below $1/N$ correspond to graphs where typically no vertices are in that block, so the effective minimum we can consider for ρ_s is $1/N$.)

To illustrate Eq. 1 of Theorem 4.2, we consider a 2-block SBM with parameters

$$B = \begin{bmatrix} 0.42 & 0.2 \\ 0.2 & 0.7 \end{bmatrix}, \qquad \rho = \begin{bmatrix} 0.5 & 0.5 \end{bmatrix}, \tag{2}$$

so that $|\{i : \tau_i = 1\}| = |\{i : \tau_i = 2\}|$ for each N. When calculating $\widehat{P}$, we omit the dimension selection step from Algorithm 2 and instead use the true dimension $d = \mathrm{rank}(B) = 2$. Fig. 3 shows $2/\rho_1$ and $1/\rho_1 + 1/\rho_2$, the scaled asymptotic RE for pairs of vertices both in block one and pairs of vertices in different blocks, respectively, in the two-block stochastic blockmodel we specified earlier. We vary ρ_1 between 0 and 1 to demonstrate how the number of pairs of vertices with the corresponding block memberships impacts the overall relative efficiency. For $N = 500$ and $M = 100$, estimates of the scaled RE based on simulations agree very closely with their corresponding theoretical values displayed in the figure. Note that when $\rho_1 = 0.5$, the scaled RE has value 4.0, which agrees with the result in Fig. 4 for simulated data.

If instead of assuming that the graphs follow an SBM distribution, we assume the graphs are distributed according to an RDPG distribution, similar gains in relative efficiency can be realized. While there is no compact analytical formula for the relative efficiency of $\widehat{P}$ versus $\bar{A}$ in the general RDPG case, using the
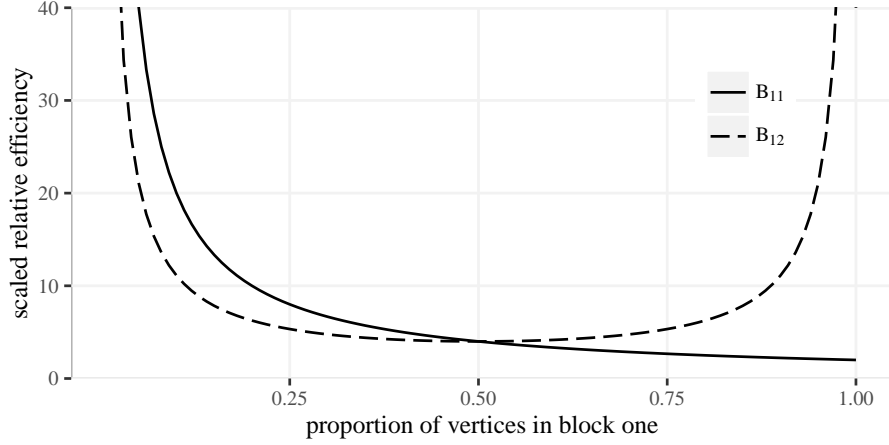
12

Fig 3: **Asymptotic scaled relative efficiency** $N \cdot \mathrm{RE}(\bar{A}, \widehat{P})$ **in a two-block SBM.** For each distinct pair of edge probabilities in a two-block SBM specified in Eq. 2, the scaled relative efficiency only depends on the proportion of vertices in each block. We show the scaled asymptotic relative efficiency as ρ_1 changes from $0, 1$ for pairs of vertices where either both are in block one or one is in block one and one is in block two. These curves all intersect at a scaled relative efficiency of 4 when $\rho_1 = 1/2 = \rho_2$. Improvements using low-rank methods are greater for larger blocks, such as for B_{11} when ρ_1 is close to 1, while the improvements are smaller for block pairs with relatively few vertex pairs such as B_{11} when ρ_1 is small and B_{12} when ρ_1 is near 0 or 1 . Note that the curve for B_{22} would be the same as that for B_{11} but reflected around the vertical line when $\rho_1 = 1/2$. Overall, $\widehat{P}$ performs best for large blocks while the improvements may be very minor for blocks with only a few vertices.

same ideas as in Theorem 4.2, we can show that $\mathrm{RE}(\bar{A}_{ij}, \widehat{P}_{ij}) = O(1/N)$. 382

Proposition 4.3. *Suppose that $A^{(1)}, A^{(2)}, \ldots, A^{(M)}$ are independently and iden-* 383
tically distributed from an RDPG distribution with common latent positions 384
$X_1, \ldots, X_n$, which are independently and identically distributed from some dis- 385
tribution. As the number of vertices $N \to \infty$, it holds for any $i \neq j$ that 386

$$\mathrm{RE}(\bar{A}_{ij}, \widehat{P}_{ij}) = O(1/N).$$

where again the asymptotic relative efficiency in N does not depend on M. 387

The proof of this proposition closely follows the proofs of Lemma 4.1 and 388
Theorem 4.2, and hence we omit it here. 389

Remark 4.4. *As we noted above, if the graphs are distributed according to* 390
an SBM or an RDPG, the relative efficiency is approximately invariant to the 391
number of graphs M when N is large. If on the other hand, the graphs are 392

generated according to a full-rank independent edge model, then the relative ef- 393
ficiency can change more dramatically as M changes. The reason for this is 394
because for larger M, more of the eigenvectors of $\bar{A}$ will begin to concentrate 395
around the eigenvectors of the mean graph. This leads to the fact that the opti- 396
mal embedding dimension for estimating the mean will increase, making $\bar{A}$ and 397
the low-rank approximation at the optimal dimension closer together. As a re- 398
sult, $\mathrm{RE}(\bar{A}, \widehat{P})$ will increase as M increases for full-rank models. Indeed, for 399
large M we could have $\mathrm{RE}(\bar{A}, \widehat{P}) \geq 1$ since we cannot guarantee that $\widehat{P}$ will 400
choose the optimal dimension. The lack of gaps in the eigenvalues of the mean 401
graph makes dimension reduction quite dangerous. In an extreme case, the low- 402
rank assumption will be mostly violated when all eigenvalues of the mean graph 403
are almost equal. This leads to a certain type of structure, which is close to 404
a constant times the identity matrix. However we don't see such structure in 405
connectomoics. We will check this in Section 4.3 when applying our estimator 406
to the CoRR dataset. 407

4.2   Finite Sample Simulations 408

In this section, we will illustrate the theoretical results from Section 3.1 re- 409
garding the relative efficiency between $\bar{A}$ and $\widehat{P}$ via Monte Carlo simulation 410
experiments in an idealized setting. These numerical simulations will also allow 411
us to investigate the finite sample performance of the two estimators. Note that 412
in Section 4.4, we will break the model assumptions slightly and run experiment 413
in a more realistic setting. 414

Here, we consider the same 2-block SBM as in Eq. 2. To be clear, we restate
the parameters here:

$$B = \begin{bmatrix} 0.42 & 0.2 \\ 0.2 & 0.7 \end{bmatrix}, \qquad \rho = \begin{bmatrix} 0.5 & 0.5 \end{bmatrix}.$$

Similarly, when calculating $\widehat{P}$, we omit the dimension selection step from Algo- 415
rithm 2 and instead use the true dimension $d = \mathrm{rank}(B) = 2$. 416

To investigate the finite sample relative efficiency, we first sample 1000 Monte 417
Carlo replicates from the above SBM distribution with different numbers of 418
vertices $N \in \{30, 50, 100, 250, 500, 1000\}$ and a fixed number of graphs $M = 100$. 419
The relative efficiency $\mathrm{RE}(\bar{A}_{ij}, \widehat{P}_{ij})$ can be estimated since P is known for this 420
simulation. Since the relative efficiency only depends on the block memberships 421
of the pair i, j, we estimate the relative efficiency for each block pair using 422

$$\widehat{\mathrm{RE}}_{st}(\bar{A}, \widehat{P}) = \frac{\sum_{\tau_i = s, \tau_j = t, i \neq j} \widehat{\mathrm{MSE}}(\widehat{P}_{ij})}{\sum_{\tau_i = s, \tau_j = t, i \neq j} \widehat{\mathrm{MSE}}(\bar{A}_{ij})}$$

for $s, t \in \{1, 2\}$, where $\widehat{\mathrm{MSE}}$ denotes the estimated mean squared error based on 423
the Monte Carlo replicates. For the remaining simulations and real data anal- 424
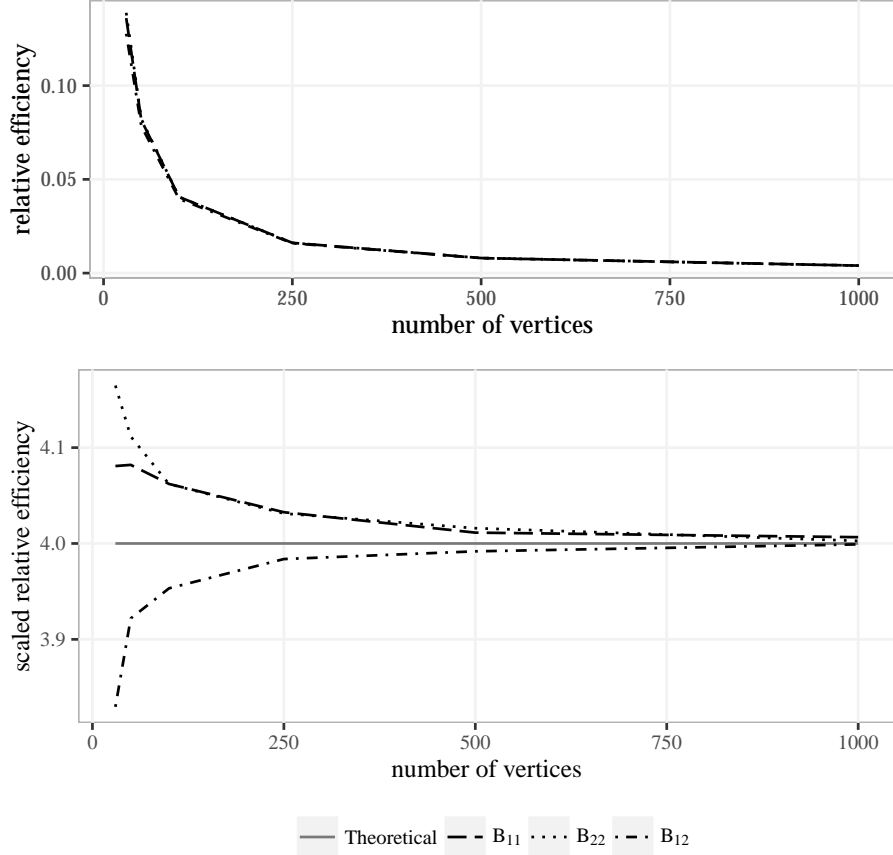ysis, we will always be considering estimated relative efficiency and estimated 425

14

Fig 4: **Finite sample relative efficiency based on simulations.** The top panel shows the estimated relative efficiency $\widehat{\mathrm{RE}}(\bar{A}, \widehat{P})$ as a function of N for fixed $M = 100$ based on simulations of an SBM. For each value of N, we used 1000 Monte Carlo replicates of the SBM from Section 4.2 to estimate the RE. Each curve corresponds to an average across vertex pairs corresponding to the three distinct block probabilities B_{11}, B_{12}, and B_{22} in the two-block SBM. Recall that values below 1 indicate that $\widehat{P}$ is performing better than $\bar{A}$. The relative efficiencies are all very close so the lines are indistinguishable.

To distinguish the three curves, the bottom panel shows the corresponding scaled relative efficiencies, $N \cdot \widehat{\mathrm{RE}}(\bar{A}, \widehat{P})$. The solid horizontal line indicates the theoretical asymptotic scaled relative which is $1/\rho_s + 1/\rho_t = 4$, since $\rho_1 = \rho_2 = 4$. All the curves converge quickly to this theoretical limit.

mean squared error rather than analytic results, and hence we will frequently   426
omit that these are estimated values when it is clear from context.   427

In Fig. 4, we plot the (estimated) relative efficiency (top panel) and the scaled   428
(estimated) relative efficiency (bottom panel), $N \cdot \widehat{\mathrm{RE}}_{st}(\bar{A}, \widehat{P})$. The different   429
dashed lines denote the RE and scaled RE associated with different block pairs,   430
either B_{11}, B_{12}, or B_{22}. As expected from Theorem 4.2, the top panel indicates   431
that the relative efficiencies are all very close together and much less than 1,   432
decreasing at the rate of $1/N$, indicating that $\widehat{P}$ is performing better than $\bar{A}$.   433

Based on Theorem 4.2, we also have that the scaled RE converges to $1/\rho_{\tau_i} +$ 434
$1/\rho_{\tau_j} = 4$ as $N \to \infty$ for all pairs i, j. This is plotted as a solid line in the   435
bottom panel. From the figure, we see that $N \cdot \widehat{\mathrm{RE}}_{st}(\bar{A}, \widehat{P})$ converges to scaled   436
asymptotic RE quite rapidly. We omit error bars as the standard errors are   437
very small for these estimates.   438

Remark 4.5. *An intriguing aspect of these finite sample results is that the*   439
scaled relative efficiencies behave differently for small graphs with fewer vertices.   440
The estimates of the edge probabilities for pairs of vertices in different blocks are   441
much better than the estimates for edges within each block. The reason for this   442
is unclear and could be due to the actual values of the true probability, but it   443
may also be due to the fact that there are approximately twice as many pairs of   444
vertices in different blocks, $N^2/4$, than there are in the same block, $N^2/8 - N/4$.   445
This could lead to an increase in effective sample size which may cause the larger   446
differences displayed in the left parts of Fig. 4. However, overall these differences   447
are nearly indistinguishable for unscaled relative efficiency.   448

4.3   CoRR Brain Graphs: Cross-Validation   449

In practice, graphs do not follow the independent edge model, let alone an   450
RDPG or SBM, but the mean of a collection of graphs is still of interest for   451
these cases. To demonstrate that the estimator $\widehat{P}$ is still useful in such cases,   452
we tested its performance on structural connectomic data. The graphs are   453
based on diffusion tensor MR images collected and available at the Consortium   454
for Reliability and Reproducibility (CoRR) [Zuo et al., 2014, Gorgolewski et al.,   455
2015] (see Section 6.3).   456

The dataset contains 454 different brain scans, each of which was processed   457
to yield an undirected, unweighted graph with no self-loops, using the pipeline   458
described in Roncal et al. [2013] and Kiar et al. [In Preparation]. The vertices   459
of the graphs represent different regions in the brain defined according to an   460
atlas. We used three atlases, the JHU atlas with 48 vertices, the Desikan atlas   461
with 70 vertices, and the CPAC200 atlas with 200 vertices. An edge exists be-   462
tween two vertices whenever there is at least one white-matter tract connecting   463
the corresponding two regions of the brain. Further details of the dataset are   464
provided in Section 6.3.   465

As discussed in Remark 4.4, we first check if the dataset has the low-rank   466
property. In Fig. 5, we plot the eigenvalues of the mean graph of all 454 graphs   467
(with diagonal augmentation) in decreasing algebraic order for three different   468

16

atlases. For all three atlases, the eigenvalues first decrease dramatically and   469
then stay around 0. So the information is mostly contained in the first few   470
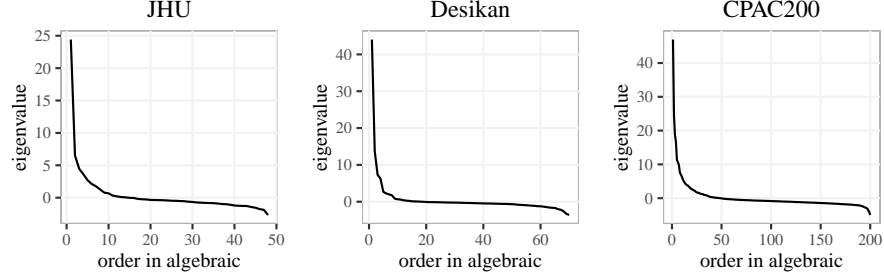dimensions. Such quasi low-rank property could be used by $\widehat{P}$ to improve $\bar{A}$.

Fig 5: **Screeplot of the population mean.** These screeplots shows the eigenvalues of the mean graph of all 454 graphs with diagonal augmentation in decreasing algebraic order for three atlases.

471

In order to evaluate the performance of the two estimators, we used a cross   472
validation on the 454 graphs of each size. Specifically, for a given atlas, each   473
Monte Carlo replicate corresponds to sampling M graphs out of the 454 and   474
computing the low-rank estimator $\widehat{P}$ and the sample mean $\bar{A}$ using the M 475
selected graphs. We then compared these estimates to the sample mean for   476
the remaining $454 - M$ adjacency matrices. While we cannot interpret this   477
mean graph as the probability matrix for an IEM distribution (see Section 4.4),   478
the sample mean for the remaining graphs does give the proportion of times   479
each pair of vertices are adjacent in the population from which the graphs were   480
sampled.   481

While in previous sections we evaluated the mean squared error for either   482
an individual entry or for an entire block in the SBM, in this section and the   483
next section we will focus on the overall error for estimating the mean graph.   484
In particular we will use the average of the mean squared error across all pairs   485
of vertices and we define $\mathrm{MSE}(\bar{A}) = \binom{N}{2}^{-1} \sum_{i>j} \mathbb{E}[\bar{A}_{ij} - P_{ij}]$ and similarly for   486
$\mathrm{MSE}(\widehat{P})$. As in the previous section, we will not use analytical evaluations of   487
the MSE and instead estimate the MSE and relative efficiencies via Monte Carlo   488
simulations.   489

We ran 1000 simulations on each of the three atlases for each sample size   490
$M = 1, 5, 10$. We also considered all possible dimensions for $\widehat{P}$ by ranging d from   491
1 to N in order to investigate the impact of the dimension selection procedures.   492
We plot $\widehat{\mathrm{MSE}}$ of $\bar{A}$ and $\widehat{P}$ in Fig. 6. The horizontal axis gives dimension d,   493
which only impacts $\widehat{P}$, which is why estimated MSE of $\bar{A}$ is shown as flat.   494

When d is small, $\widehat{P}$ underestimates the dimension and throws away impor-   495
tant information, which leads to relatively poor performance. When $d = N$, $\widehat{P}$ 496
is equal to $\bar{A}$, so that the curve for $\widehat{\mathrm{MSE}}$ for $\widehat{P}$ ends at $\widehat{\mathrm{MSE}}(\bar{A})$. In practice, we   497
use algorithms like Zhu and Ghodsi's method or USVT to select the dimension   498

17

d (see Section 6.1). In the figure, we denote the 3rd elbow found by the Zhu and Ghodsi method by a triangle, and denote the dimension selected by USVT with threshold 0.7 by a square. Both dimension selection algorithms tend to select dimensions which nearly minimize the mean squared error.

When M is 1 or 5, $\bar{A}$ has large variance which leads to large $\widehat{\mathrm{MSE}}$. Meanwhile, $\widehat{P}$ reduces the variance by taking advantages of inherent low-rank structure of the mean graph. Such smoothing effect is especially obvious while we only have 1 observation. When $M = 1$, all weights of the graph are either 0 or 1, leading to a very bumpy estimate $\bar{A}$. In this case, $\widehat{P}$ smooth the connectomes estimate and improve the performance. Additionally, we see that there is a large range of dimensions where the performance for $\widehat{P}$ is superior to $\bar{A}$. With a larger M, the performance of $\bar{A}$ improves so that its performance is frequently superior but nearly identical to $\widehat{P}$.

For a more specific comparison of the performance of $\widehat{P}$ and $\bar{A}$ in the most realistic situation where the rank d must be chosen based on data, Table 1 shows estimated relative efficiencies of $\widehat{P}$ versus $\bar{A}$. For each atlas and each sample size, we compare the Zhu and Ghodsi method [Zhu and Ghodsi, 2006] with the USVT method [Chatterjee, 2015] and note that both perform reasonably well relative to the full-dimensional $\bar{A}$. We omit confidence intervals for the estimated relative efficiencies since all confidence intervals had lengths less than 0.015, indicating that all relative efficiencies, aside from the relative efficiency for the CPAC200 atlas at $M = 10$, are very different from 1.

Again we can see that the largest improvements using $\widehat{P}$ occur when m is small and N is large. On the other hand, once $M = 10$, $\bar{A}$ tends to do nearly as well or better than $\widehat{P}$. Nonetheless, when applied to subgroups inference, such as all females between the age of 21 and 25, $\widehat{P}$ can be really helpful for better exploring differences between groups compared to $\bar{A}$ due to a small sample size of each subgroup. In addition, $\widehat{P}$ offers certain advantages, especially since low-rank estimates can often be more easily interpretable by considering the latent position representation described in Section 2.3.

To further illustrate the differences between the two estimators, we considered a single random sample of size $M = 5$ based on the Desikan atlas. We calculated $\bar{A}$ and $\widehat{P}$, using Zhu and Ghodsi's 3rd elbow to select $d = 11$. In Fig. 1, the estimates $\bar{A}$ and $\widehat{P}$ as well as the sample mean of 454 graphs (as a close estimate of P) are plotted. Since the sample size is small, there are a lot of pairs of vertices with no edges or 5 edges in the 5 observations. This leads to the white and black pixels in the image corresponding to $\bar{A}$. On the other hand, $\widehat{P}$ has a finer gradient of values which in this case leads to a more accurate estimate.

Moreover, Fig. 7 shows the values for the absolute estimation error $|\bar{A} - P|$ and $|\widehat{P} - P|$. The lower triangular sections show the actual absolute difference while the upper triangular matrix highlights the vertex pairs with absolute differences larger than 0.4. There are 18 edges from $\bar{A}$ and 6 edges from $\widehat{P}$ being highlighted in the figure, further indicating the superior performance of $\widehat{P}$. Note that approximately 13% of all pairs of vertices are adjacent in all 454 graphs
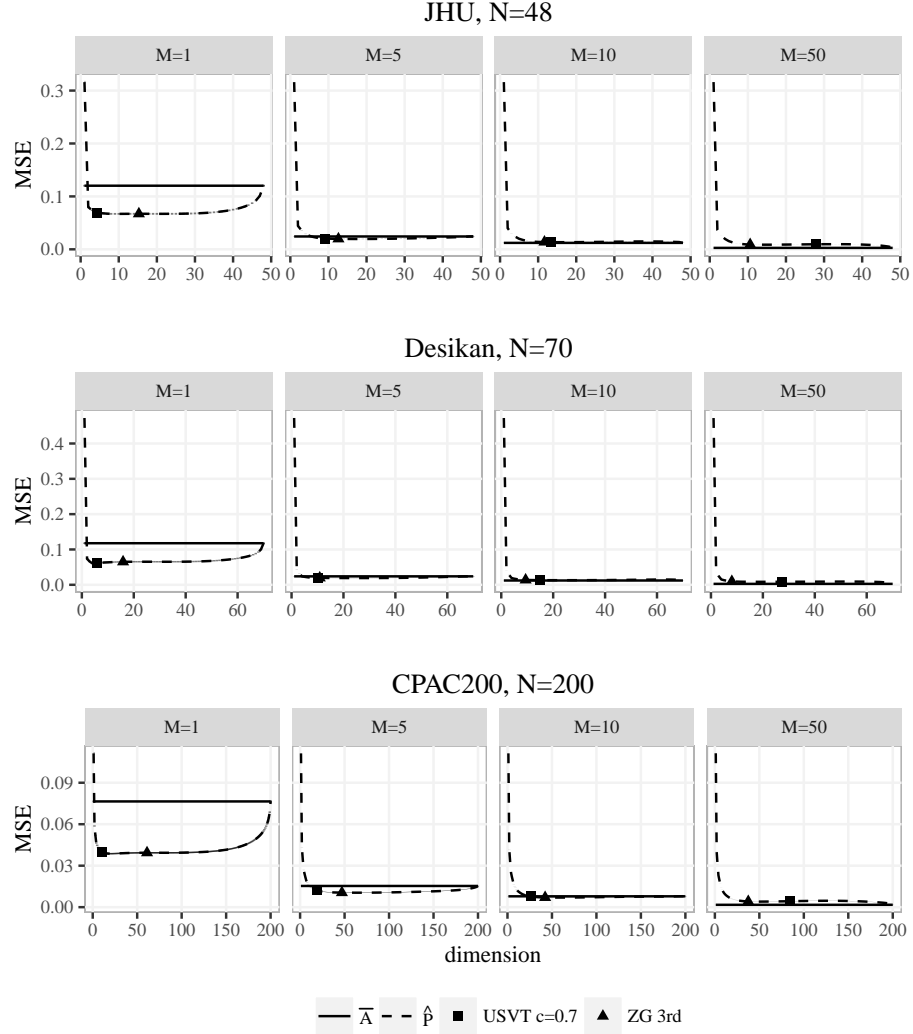
18

Fig 6: **Comparison of $\widehat{\mathrm{MSE}}$ of $\widehat{P}$ and $\bar{A}$ for three atlases at three sample sizes for the CoRR data.** These plots show the mean squared error for $\bar{A}$ (solid line) and $\widehat{P}$ (dashed line) for three dataset (JHU, Desikan, and CPAC200) while embedding the graphs into different dimensions and with different sample sizes M. The average dimensions chosen by the 3rd elbow of Zhu and Ghodsi is denoted by a triangle and those chosen by USVT with threshold equaling 0.7 is denoted by a square. Vertical intervals, visible mainly in the $N = 48, 70$ and $M = 1$ plots, represent the 95% confidence interval for the mean squared errors. When M is small, $\widehat{P}$ outperforms $\bar{A}$ with a flexible range of the embedding dimension including the average of the dimensions selected by Zhu and Ghodsi and USVT.

JHU	$M = 1$	$M = 5$	$M = 10$
ZG	0.54	0.81	1.14
USVT	0.56	0.84	1.12
Desikan	$M = 1$	$M = 5$	$M = 10$
ZG	0.52	0.81	1.14
USVT	0.50	0.81	1.09
CPAC200	$M = 1$	$M = 5$	$M = 10$
ZG	0.51	0.68	0.89
USVT	0.52	0.79	0.99

Table 1: **Relative efficiencies of $\bar{A}$ versus $\widehat{P}$ for the CoRR data set.** For each atlas, JHU, Desikan, and CPAC 200, we sampled graphs which we used to compute $\bar{A}$ and $\widehat{P}$. We compared different sample sizes M and different dimension selection procedures, ZG and USVT. For each of the two methods for computing $\widehat{P}$, we estimated their relative efficiencies with respect to the sample mean $\bar{A}$. Confidence intervals all had lengths less than 0.015, and hence we omitted them for clarity. Overall, the relative efficiencies are greater for smaller sample sizes M and larger number of vertices N.

and hence $\bar{A}$ will always have zero error for those pairs of vertices. Nonetheless, $\widehat{P}$ typically outperforms $\bar{A}$.

To investigate the difference in performance with respect to the geometry of the brain, in Fig. 8 we plot the 50 edges with the largest differences $|\bar{A}_{ij} - P_{ij}| - |\widehat{P}_{ij} - P_{ij}|$ according to the location of the corresponding regions in the brain. Red edges indicate that $\widehat{P}$ overestimates P, while blue means that $\widehat{P}$ underestimates P. The edge width is determined by the estimation error for $\widehat{P}$, where pairs with larger estimation error are represented by thicker lines. We also highlight the five regions corresponding to vertices that contribute most to the difference, meaning the vertices i with the largest value of $\sum_j(|\bar{A}_{ij} - P_{ij}| - |\widehat{P}_{ij} - P_{ij}|)$. Notably, three of these top five regions form a contiguous group of regions. The top five regions are the inferior temporal, middle temporal, and transverse temporal regions in the left hemisphere and the parahippocampal and parsopercularis regions in the right hemisphere of the Desikan atlas.

These results demonstrate that for small sample sizes, such as $M = 1$ or $M = 5$, and for the atlases with a larger number of vertices, $\widehat{P}$ gives a better estimate than $\bar{A}$ for the CoRR dataset. Importantly, this improvement is robust to the embedding dimension provided the dimension is not underestimated. We should note that though the total error for $\widehat{P}$ is smaller in this case, for certain entries $\bar{A}$ does perform better. For example, there are some pairs of vertices that are adjacent for all samples in the population and for these pairs $\bar{A}$ will always perform better than $\widehat{P}$.
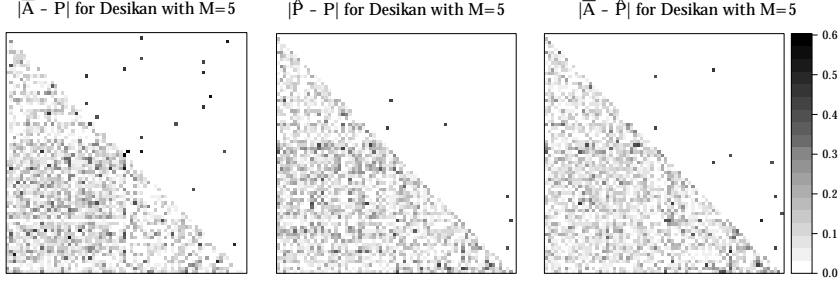
Fig 7: **Heat plot of absolute estimation error for $\bar{A}$ and $\widehat{P}$ (lower triangle) and absolute errors above 0.4 (upper triangle).** These heat plots show the absolute estimation error $|\bar{A}-P|$ and $|\widehat{P}-P|$ for a sample of size $M=5$ from the Desikan dataset. The embedding dimension for $\widehat{P}$ is $d=11$ selected by the 3rd elbow of the ZG method. The lower triangular matrix shows the actual absolute difference, while the upper triangular matrix only highlights the edges with absolute differences larger than 0.4. The fact that 18 edges from $\bar{A}$ are highlighted and only six edges from $\widehat{P}$ are highlighted indicates that $\widehat{P}$ has fewer large outliers compared to $\bar{A}$.
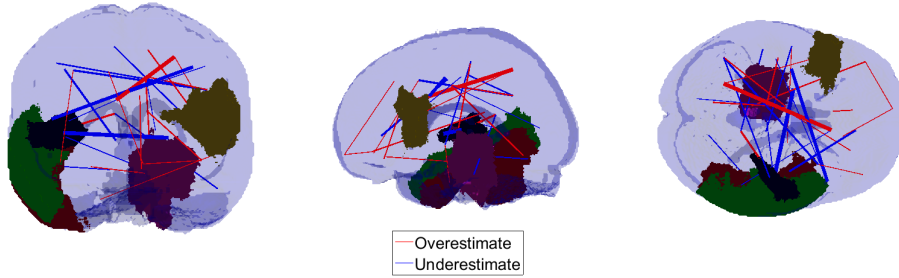

Fig 8: **Top 5 regions of the brain (vertices in graphs) and top 50 connections between regions (edges in graphs) with the largest differences $|\bar{A}_{ij}-P_{ij}|-|\widehat{P}_{ij}-P_{ij}|$.** Red edges indicate that $\widehat{P}$ overestimate P while blue means that $\widehat{P}$ underestimates P. The edge width is determined by the estimation error. Connections with larger estimation error are represented by thicker lines. This figure shows the regions and connections of the brain where $\widehat{P}$ outperforms $\bar{A}$ the most for estimating P.

21

4.4 Synthetic Data Analysis for Full Rank IEM

While the theory we have developed is based on the assumption that the mean graph is low rank, as we have seen in Section 4.3, $\widehat{P}$ often performs well even when this assumption is false. To further illuminate this point, we performed a synthetic data analysis under a full-rank independent edge model where we used the sample mean of the 454 graphs in the Desikan dataset as the probability matrix P. As in the previous section, we simulated datasets of size $M = 1, 5,$ and 10 and used $\bar{A}$ and $\widehat{P}$, where we varied the rank of $\widehat{P}$ from 1 to 70.

Fig. 9 shows the resulting estimated MSE for $\bar{A}$ (solid line) and $\widehat{P}$ (dashed line) for simulated data based on the full rank probability matrix P shown in the left panel of Fig. 1. We see that the results are very similar to those presented in Section 4.3, though overall $\widehat{P}$ performs even better than in the real data experiments. When M is small, $\widehat{P}$ outperforms $\bar{A}$ with a flexible range of the embedding dimension including those selected by the Zhu and Ghodsi method. On the other hand, when M is large enough, both estimators perform well with the decision between the two being less conclusive. This simulation again shows the robustness of $\widehat{P}$ to deviations from the RDPG model, specifically if the probability matrix is full-rank.

We also note that the finite-sample relative efficiency in these cases shows is even more favorable to $\widehat{P}$, with relative efficiencies lower than $1/3$ for $M = 1$, than for the real data, where relative efficiencies were at best around $1/2$ for $M = 1$. From this observation, we can postulate that the degradation in the performance of $\widehat{P}$ in real data can at least partially be attributed to the fact that the independent edge assumption does not hold for real data.

5 Discussion

Motivated by the RDPG model, our methodology takes advantage of the low-rank structure of the graphs by applying low-rank approximation to the entry-wise MLE. We give a closed form for the asymptotic relative efficiency between the entry-wise MLE $\bar{A}$ and our estimator $\widehat{P}$ in the case of a stochastic block-model, demonstrating that when the number of vertices N is sufficiently large, low-rank methods provide a substantial improvement. In particular, we show that for a stochastic blockmodel with fixed number of blocks K, block size proportion ρ, and number of graphs M, the low-rank estimator $\widehat{P}$ has MSE which is on the order of N times lower than the MSE for $\bar{A}$.

Moreover, our estimator outperforms the entry-wise MLE in a cross validation analysis of the CoRR brain graphs and in low- and full-rank simulation settings. These results illustrate that $\widehat{P}$ performs well even when the low-rank assumption is violated and that $\widehat{P}$ is robust and can be applied in practice.

One of the key observations from our real data analysis was that the largest improvements using the low-rank method occurred when the number of graphs M was small, and that it provided only minor improvements or even degraded performance slightly when M was large. However, even in large scale studies the
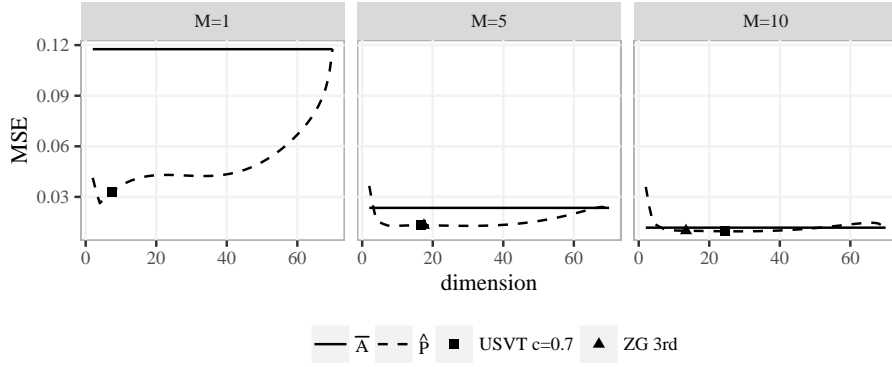
Fig 9: **Comparison of $\widehat{P}$ and $\bar{A}$ for synthetic data analysis.** As in Fig. 4, this figure shows $\widehat{\text{MSE}}$ for $\bar{A}$ (solid line) and $\widehat{P}$ (dashed line) for simulated data with different sample sizes M based on the sample mean for the Desikan dataset. Again, the average of dimensions selected by the USVT method (square) and the ZG method (triangle) tend to nearly approximate the optimal dimension. Overall, we see that the structure of these plots well approximates the structure for the real data indicating that performance for the independent edge model will tend to translate in structure to non-independent edge scenarios. On the other hand, the relative efficiency $\widehat{\text{RE}}(\bar{A}, \widehat{P})$ is lower for this synthetic data analysis than for the CoRR data.

low-rank methods will be useful for estimating graph means for subpopulations, e.g. the population of females over 60 with some college education. Using the element-wise sample mean for such small strata, which may have fewer than ten subjects, will frequently result in a degradation of performance. Similarly, Durante et al. [2014] used low-rank deviations from a full rank population mean to model collections of graphs and our methods could be easily adapted to those ideas.

We also note that low-rank methods can often be more easily interpreted. By representing a low-rank matrix in terms of the latent position, where each vertex is represented as a vector in $\mathbb{R}^d$ and the entries of the matrix are given by the inner products of these vectors (see Section 2.3), one can analyze and visualize the geometry of these vectors in order to interpret how each vertex is behaving in the context of the larger graph. Additionally, such a representation allows the use of techniques from multivariate analysis to further study the estimated population mean.

While the low-rank methods considered in this paper will often offer substantial improvements, further refinements of these methods which account for the particular traits of connectomics data would be useful to improve estimation further. For example, we assume that the adjacency matrix is observed without contamination, however in practice there will be noise in the observed graph and one may seek to account for this noise with more robust methods. This may be especially fruitful when each graph has weighted edges and the weights themselves have noisy or heavy-tailed distributions. Rank-based methods and robust likelihood methods could be very useful in that case [Huber and Ronchetti, 2009, Qin and Priebe, 2013].

Another issue that arose in our analysis of the connectome dataset was the presence of structural ones in the mean graph for the population. These structural ones appear since edges between certain regions of the brain are present in all or nearly all members of the healthy population. The low-rank methods tend to miss these always-present edges while the sample mean will always capture them. Detecting and incorporating structural ones and zeros could yield methods that share the best elements of both methods considered here.

For the CoRR dataset, we used a cross-validation framework where we compared the estimates based on a subsample to the mean for the held-out set. Another option would be to compare the estimates $\bar{A}$ and $\widehat{P}$ to the mean for the entire population including the subsample. Both of these analyses lead to very similar results in the cases presented above, but for various reasons one may prefer one analysis over another. The cross-validation method is most reasonable from a prediction perspective where prediction about new samples is of interest. If instead one is interested in learning directly about the mean of a population, especially a finite population, the sub-sampling approach may be the most logical choice.

6 Methods

6.1 Choosing Dimension

Often in dimensionality reduction techniques, the choice for dimension d, relies on analyzing the set of the ordered eigenvalues, looking for a "gap" or "elbow" in the scree-plot. Zhu and Ghodsi [2006] present an automated method for finding this gap in the scree-plot that takes only the ordered eigenvalues as an input and uses Gaussian mixture modeling to find these gaps. The mixture modeling results in multiple candidate dimensions or elbows, and our analysis indicated that underestimating the dimension is much more harmful than overestimating the dimension. For this reason, we used the 3rd elbow in the experiments performed for this work.

Universal Singular Value Thresholding (USVT) is a simple estimation procedure proposed in Chatterjee [2015] that can work for any matrix that has "a little bit of structure". In our setting, it selects the dimension d as the number of singular values that are greater than a constant c times $\sqrt{N/M}$. The specific constant c must be selected carefully based on the mean and variance of the entries, and since again we found that overestimating the dimension was not overly harmful, we chose a relatively small value of $c = 0.7$.

Overall, selecting the appropriate dimension is a challenging task and numerous methods could be applied successfully depending on the setting. On the other hand, we have observed that in our setting, many dimensions will yield nearly optimal mean squared errors. Thus efforts to ensure the selected dimension is in the appropriate range are more important than finding the best dimension.

6.2 Graph Diagonal Augmentation

The graphs examined in this work have no self-loops and thus the diagonal entries of the adjacency matrix and the mean graph are all zero. However, when computing the low-rank approximation, these structural zeros lead to increased errors in the estimation of the mean graph. While this problem has been investigated in the single graph setting, with multiple graphs, the problem is exacerbated since the variance of the other entries is lower, so the relative impact of the bias in the diagonal entries is higher. Moreover, the sum of eigenvalues of the hollow matrix will be zero, leading to an indefinite matrix, which violates the positive semi-definite assumption. So it is important to remedy the situation that we don't observe the diagonal entries.

Marchette et al. [2011] proposed the simple method of imputing the diagonals to be equal to the average of the non-diagonal entries for the corresponding row. Earlier, Scheinerman and Tucker [2010] proposed using an iterative method to impute the diagonal entries. In this work, we combine these two ideas by first using the row-average method (see Step 3 of Algorithm 2) and then using one step of the iterative method (see Step 6 of Algorithm 2). Note that when computing errors, we omit the diagonal entries since these are known to be

zero.

6.3 Dataset Description

The original dataset is from the Emotion and Creativity One Year Retest
Dataset provided by Qiu, Zhang and Wei from Southwest University available
at the Consortium for Reliability and Reproducibility (CoRR) [Zuo et al., 2014,
Gorgolewski et al., 2015]. It is comprised of 235 subjects, all of whom were
college students. Each subject underwent two sessions of anatomical, resting
state DTI scans, spaced one year apart. Due to incomplete data, only 454 scans
are available.

When deriving MR connectomes, the NeuroData team parcellates the brain
into groups of voxels as defined by anatomical atlases [neu, Kiar, 2016]. The at-
lases are defined either physiologically by neuroanatomists (Desikan and JHU),
or are generated using an automated segmentation algorithm (CPAC200). Once
the voxels in the original image space are grouped into regions, an edge is placed
between two regions when there is at least one white-matter tract, derived using
a tractography algorithm, connecting the corresponding two parts of the brain.
The resulting graphs are undirected, unweighted, and have no self-loops.

6.4 Outline for the Proof of the Theorems

Here we provide an outline of the proof of Lemma 4.1 which provides the ap-
proximate MSE of $\widehat{P}$ in the stochastic blockmodel case. The result depends on
using the asymptotic results for the distribution of eigenvectors from Athreya
et al. [2013] which extend to the multiple graph setting in a straightforward
way.

The first key observation is that since $\bar{A}$ is computed from iid observations
each with expectation P, $\bar{A}$ is unbiased for P and $\mathrm{Var}(A_{ij}) = \frac{1}{M}P_{ij}(1 - P_{ij})$.
The results of Athreya et al. [2013] provide a central limit theorem for estimates
of the latent position in an RDPG model for a single graph. Since the variance of
each entry is scaled by $1/M$ in $\bar{A}$, the analogous result for $\bar{A}$ is that the estimated
latent positions will follow an approximately normal distribution with variance
scaled by $1/M$ compared to the variance for a single graph.

Since $\widehat{P}_{ij} = \widehat{X}_i^\top \widehat{X}_j$ is a noisy version of the dot product of $\nu_s^\top \nu_t$ from
Section 2.3 and each $\widehat{X}_i$ is approximately independent and normal, we can
use common results for the variance of the inner product of two independent
multivariate normals [Brown and Rutemiller, 1977]. After simplifications that
occur in the stochastic blockmodel setting, we can derive that the variance of
$\widehat{P}_{ij}$ converges to $\left(1/\rho_{\tau_i} + 1/\rho_{\tau_j}\right) P_{ij}(1 - P_{ij})/(N \cdot M)$ as $N \to \infty$. Since the
variance of $\bar{A}_{ij}$ is $P_{ij}(1 - P_{ij})/M$, the relative efficiency between $\widehat{P}_{ij}$ and $\bar{A}_{ij}$ is
approximately $(\rho_{\tau_i}^{-1} + \rho_{\tau_j}^{-1})/N$ when N is sufficiently large.

26

Acknowledgments

References

Neurodata's mri to graphs pipeline. `http://m2g.io`. Accessed: 2016-05-23.

Christophe Ambroise and Catherine Matias. New consistent and asymptotically normal parameter estimates for random-graph mixture models. *Journal of the Royal Statistical Society: Series B (Statistical Methodology)*, 74(1):3–35, 2012.

Avanti Athreya, CE Priebe, M Tang, V Lyzinski, DJ Marchette, and DL Sussman. A limit theorem for scaled eigenvectors of random dot product graphs. *Sankhya A*, pages 1–18, 2013.

Béla Bollobás, Svante Janson, and Oliver Riordan. The phase transition in inhomogeneous random graphs. *Random Structures & Algorithms*, 31(1):3–122, 2007.

Gerald G Brown and Herbert C Rutemiller. Means and variances of stochastic vector products with applications to random linear models. *Management Science*, 24(2):210–216, 1977.

Sourav Chatterjee. Matrix estimation by universal singular value thresholding. *The Annals of Statistics*, 43(1):177–214, 2015.

David S Choi, Patrick J Wolfe, and Edoardo M Airoldi. Stochastic blockmodels with a growing number of classes. *Biometrika*, page asr053, 2012.

J-J Daudin, Franck Picard, and Stéphane Robin. A mixture model for random graphs. *Statistics and computing*, 18(2):173–183, 2008.

Daniele Durante, David B Dunson, and Joshua T Vogelstein. Nonparametric bayes modeling of populations of networks. *arXiv preprint arXiv:1406.7851*, 2014.

Cedric E Ginestet, Prakash Balanchandran, Steven Rosenberg, and Eric D Kolaczyk. Hypothesis testing for network data in functional neuroimaging. *arXiv preprint arXiv:1407.5525*, 2014.

Krzysztof J Gorgolewski, Natacha Mendes, Domenica Wilfling, Elisabeth Wladimirow, Claudine J Gauthier, Tyler Bonnen, Florence JM Ruby, Robert Trampel, Pierre-Louis Bazin, Roberto Cozatl, et al. A high resolution 7-tesla resting-state fmri test-retest dataset with cognitive and physiological measures. *Scientific data*, 2, 2015.

Sam Gutmann. Stein's paradox is impossible in problems with finite sample space. *The Annals of Statistics*, pages 1017–1020, 1982.

Peter D Hoff, Adrian E Raftery, and Mark S Handcock. Latent space approaches to social network analysis. *Journal of the american Statistical association*, 97 (460):1090–1098, 2002.

Paul W Holland, Kathryn Blackmond Laskey, and Samuel Leinhardt. Stochastic blockmodels: First steps. *Social networks*, 5(2):109–137, 1983.

Peter J. Huber and Elvezio M. Ronchetti. *Robust statistics.* Wiley Series in Probability and Statistics. John Wiley & Sons, Inc., Hoboken, NJ, second edition, 2009. ISBN 978-0-470-12990-6.

W. James and Charles Stein. Estimation with quadratic loss. In *Proceedings of the Fourth Berkeley Symposium on Mathematical Statistics and Probability, Vol. I*, pages 361–379. Univ. California Press, Berkeley, Calif., 1961.

Xiaoyi Jiang, Andreas Müunger, and Horst Bunke. On median graphs: Properties, algorithms, and applications. *IEEE Transactions on Pattern Analysis and Machine Intelligence*, 23(10):1144–1151, 2001.

Gregory Kiar. Gremlin: Graph estimation from mr images leading to inference in neuroscience. 2016.

Gregory Kiar, William Gray Roncal, Disa Mhembere, Eric Bridgeford, Randal Burns, Carey Priebe, and Joshua T. Vogelstein. m2g: A reliable and robust open-source one-click pipeline for mri to graph connectome estimation. In Preparation.

David Marchette, Carey Priebe, and Glen Coppersmith. Vertex nomination via attributed random dot product graphs. In *Proceedings of the 57th ISI World Statistics Congress*, volume 6, page 16, 2011.

Christine Leigh Myers Nickel. *Random dot product graphs: A model for social networks*, volume 68. 2007.

Dragana M Pavlovic, Petra E Vértes, Edward T Bullmore, William R Schafer, and Thomas E Nichols. Stochastic blockmodeling of the modules and core of the caenorhabditis elegans connectome. *PloS one*, 9(7):e97584, 2014.

Franck Picard, Vincent Miele, Jean-Jacques Daudin, Ludovic Cottret, and Stéphane Robin. Deciphering the connectivity structure of biological networks using mixnet. *BMC bioinformatics*, 10(6):1, 2009.

Yichen Qin and Carey E Priebe. Maximum l q-likelihood estimation via the expectation-maximization algorithm: A robust estimation of mixture models. *Journal of the American Statistical Association*, 108(503):914–928, 2013.

W. Gray Roncal, Z. H. Koterba, D. Mhembere, D. M. Kleissas, J. T. Vogelstein, R. Burns, A. R. Bowles, D. K. Donavos, S. Ryman, R. E. Jung, L. Wu, V. Calhoun, and R. J. Vogelstein. Migraine: Mri graph reliability analysis and inference for connectomics. In *Global Conference on Signal and Information Processing (GlobalSIP), 2013 IEEE*, pages 313–316, Dec 2013.

Edward R Scheinerman and Kimberly Tucker. Modeling graphs using dot product representations. *Computational Statistics*, 25(1):1–16, 2010.

Charles Stein. Inadmissibility of the usual estimator for the mean of a multivariate normal distribution. In *Proceedings of the Third Berkeley Symposium on Mathematical Statistics and Probability, vol. I*, pages 197–206. University of California Press, Berkeley and Los Angeles, 1956.

Daniel L Sussman, Minh Tang, and Carey E Priebe. Consistent latent position estimation and vertex classification for random dot product graphs. *IEEE transactions on pattern analysis and machine intelligence*, 36(1):48–57, 2014.

G. V. Trunk. A problem of dimensionality: A simple example. *Pattern Analysis and Machine Intelligence, IEEE Transactions on*, (3):306–307, 1979.

Patrick J Wolfe and Sofia C Olhede. Nonparametric graphon estimation. *arXiv preprint arXiv:1309.5936*, 2013.

Stephen J Young and Edward R Scheinerman. Random dot product graph models for social networks. In *Algorithms and models for the web-graph*, pages 138–149. Springer, 2007.

Hugo Zanghi, Christophe Ambroise, and Vincent Miele. Fast online graph clustering via erdős–rényi mixture. *Pattern Recognition*, 41(12):3592–3599, 2008.

Hugo Zanghi, Stevenn Volant, and Christophe Ambroise. Clustering based on random graph model embedding vertex features. *Pattern Recognition Letters*, 31(9):830–836, 2010.

Mu Zhu and Ali Ghodsi. Automatic dimensionality selection from the scree plot via the use of profile likelihood. *Computational Statistics & Data Analysis*, 51(2):918–930, 2006.

Xi-Nian Zuo, Jeffrey S Anderson, Pierre Bellec, Rasmus M Birn, Bharat B Biswal, Janusch Blautzik, John CS Breitner, Randy L Buckner, Vince D Calhoun, F Xavier Castellanos, et al. An open science resource for establishing reliability and reproducibility in functional connectomics. *Scientific data*, 1, 2014.

A Proofs for Theory Results

Here we present the proofs of the results in Section 4.1. To keep the ideas clear and concise, we leave out some details which are only slight changes to previous works. We assume the block memberships τ_i are drawn iid from a categorical distribution with block membership probabilities given by $\rho \in [0,1]^K$ where $\sum_i \rho_i = 1$. We will also assume that for a given N, the block memberships are fixed for all graphs.

Denote matrix of between-block edge probabilities by $B = \nu\nu^\top \in [0,1]^{K \times K}$ which we assume has rank K and is positive definite. By definition, the mean of the collection of graphs generated from this SBM is P, where $P_{ij} = B_{\tau_i, \tau_j}$.

We observe M graphs on N vertices $A^{(1)}, \cdots, A^{(M)}$ sampled independently from the SBM conditioned on τ. Define $\bar{A} = \frac{1}{M} \sum_{t=1}^{M} A^{(t)}$. Let $\widehat{U}\widehat{S}\widehat{U}^\top$ be the best rank-d positive semidefinite approximation of $\bar{A}$, then we define $\widehat{P} = \widehat{X}\widehat{X}^\top$, where $\widehat{X} = \widehat{U}\widehat{S}^{1/2}$.

The proofs presented here will rely on a central limit theorem developed in Athreya et al. [2013]. We modify the theorem slightly to account for the multiple graph setting and present it in the special case of the stochastic blockmodel.

Theorem A.1 (Corrolary of Theorem 1 in Athreya et al. [2013]). *In the setting above, let $X = [X_1, \ldots, X_N]^\top \in \mathbb{R}^{K \times d}$ have row i equal to $X_i = \nu_{\tau_i}$ (recall that τ_i are drawn from $[K]$ according to the probabilities ρ). Then there exists an orthogonal matrix W such that for each row i and j and any $z \in \mathbb{R}^d$, conditioned on $\tau_i = s$ and $\tau_j = t$,*

$$\Pr\left\{ \sqrt{n}(W\widehat{X}_i - \nu_s) \leq z, \sqrt{n}(W\widehat{X}_j - \nu_t) \leq z' \right\} = \Phi(z, \Sigma(\nu_s)/M)\Phi(z', \Sigma(\nu_t)/M) + o(1)$$

(3)

where $\Sigma(x) = \Delta^{-1}\mathbb{E}[X_j X_j^\top (x^\top X_j - (x^\top X_j)^2)]\Delta^{-1}$ and $\Delta = \mathbb{E}[X_1 X_1^T]$ is the second moment matrix, with all expectations taken unconditionally. The function Φ is the cumulative distribution function for a multivariate normal with mean zero and the specified covariance, and $o(1)$ denotes a function that tends to zero as $N \to \infty$.

The proof of this result follows very closely the proof of the result in the original paper with only slight modifications for the multiple graph setting.

We now prove a technical Lemma which yields the simplified form for the variance under the stochastic blockmodel.

Lemma A.2. *In the same setting as Theorem 4.2, for any $1 \leq s, t \leq K$, we have*

$$\nu_s^\top \Sigma(\nu_t)\nu_s = \frac{1}{\rho_s}\nu_s^\top \nu_t \ (1 - \nu_s^\top \nu_t).$$

Proof. Under the stochastic blockmodel with parameters (B, ρ), we have $X_i \overset{iid}{\sim} \sum_{k=1}^{K} \rho_k \delta_{\nu_k}$, where $\nu = [\nu_1, \cdots, \nu_K]^\top$ satisfies $B = \nu\nu^\top$. Without loss of generality, we could assume that $\nu = US$ where $U = [u_1, \cdots, u_K]^\top$ is orthonormal

in columns and S is a diagonal matrix. Here we can conclude that $\nu_s^\top = u_s^\top S$. Defining $R = \mathrm{diag}(\rho_1, \cdots, \rho_K)$, we have

$$\Delta = \mathbb{E}[X_1 X_1^\top] = \sum_{k=1}^{K} \rho_k \nu_k \nu_k^\top = \nu^\top R \nu = SU^\top RUS.$$

Thus

$$
\begin{aligned}
\nu_s^\top \Sigma(\nu_t)\nu_s &= \nu_s^\top \Delta^{-1} \sum_{k=1}^{K} \rho_k \nu_k \nu_k^\top (\nu_t^\top \nu_k)(1 - \nu_t^\top \nu_k)\Delta^{-1}\nu_s \\
&= \sum_{k=1}^{K} \rho_k (\nu_s^\top \Delta^{-1}\nu_k)(\nu_k^\top \Delta^{-1}\nu_s)(\nu_t^\top \nu_k)(1 - \nu_t^\top \nu_k) \\
&= \sum_{k=1}^{K} \rho_k (u_s^\top U^\top R^{-1} U u_k)^2 (\nu_t^\top \nu_k)(1 - \nu_t^\top \nu_k) \\
&= \sum_{k=1}^{K} \rho_k (e_s^\top R^{-1} e_k)^2 (\nu_t^\top \nu_k)(1 - \nu_t^\top \nu_k) \\
&= \sum_{k=1}^{K} \rho_k \delta_{sk} \rho_s^{-2} (\nu_t^\top \nu_k)(1 - \nu_t^\top \nu_k) \\
&= \frac{1}{\rho_s} \nu_t^\top \nu_s (1 - \nu_t^\top \nu_s)
\end{aligned}
$$

$\square$

Lemma A.3 (Lemma 4.1). *In the same setting as above, for any i, j, conditioning on $X_i = \nu_{\tau_i}$ and $X_j = \nu_{\tau_j}$, we have*

$$\lim_{N \to \infty} N \cdot \mathrm{Var}(\widehat{P}_{ij}) = \frac{1/\rho_{\tau_i} + 1/\rho_{\tau_j}}{M} P_{ij}(1 - P_{ij}).$$

And for N large enough, conditioning on $X_i = \nu_{\tau_i}$ and $X_j = \nu_{\tau_j}$, we have

$$\mathbb{E}[(\widehat{P}_{ij} - P_{ij})^2] \approx \frac{1/\rho_{\tau_i} + 1/\rho_{\tau_j}}{MN} P_{ij}(1 - P_{ij}).$$

Proof. Conditioned on $X_i = \nu_k$, we have by Theorem A.1,

$$\mathbb{E}[W\widehat{X}_i] = \nu_k + o(1)$$

and

$$n \cdot \mathrm{Cov}(W\widehat{X}_i, W_n\widehat{X}_i) = \Sigma(\nu_k)/M.$$

Also, Corollary 4.11 in Athreya et al. [2013] says $\widehat{X}_i$ and $\widehat{X}_j$ are asymptotically independent. Thus, conditioning on $X_i = \nu_s$ and $X_j = \nu_t$, we have $\lim_{n \to \infty} \mathbb{E}[\widehat{X}_i^\top \widehat{X}_j] = \lim_{n \to \infty} \mathbb{E}[(W_n\widehat{X}_i)^\top]\mathbb{E}[W_n\widehat{X}_j] = \nu_s^\top \nu_t = P_{ij}$.

Since $\widehat{P}_{ij} = \widehat{X}_i^\top \widehat{X}_j$ is a noisy version of the dot product of $\nu_s^\top \nu_t$, combined with Lemma A.2 and the results above, by Equation 5 in Brown and Rutemiller (1977), conditioning on $X_i = \nu_s$ and $X_j = \nu_t$, we have

$$\mathbb{E}[\widehat{X}_i^\top \widehat{X}_j] = \mathbb{E}[(W_n \widehat{X}_i)^\top] \mathbb{E}[W_n \widehat{X}_j] = \nu_s^\top \nu_t + o(1) = P_{ij} + o(1)$$

and

$$
\begin{aligned}
&N \cdot \mathrm{Var}(\widehat{P}_{ij}) \\
=& \frac{1}{M} \left(\nu_s^\top \Sigma(\nu_t) \nu_s + \nu_t^\top \Sigma(\nu_s) \nu_t^\top \right) + \frac{1}{M^2 N} \left(tr(\Sigma(\nu_s) \Sigma(\nu_t)) \right) + o(1) \\
=& \frac{1}{M} \left(\nu_s^\top \Sigma(\nu_t) \nu_s + \nu_t^\top \Sigma(\nu_s) \nu_t^\top \right) + o(1) \\
=& \frac{1/\rho_s + 1/\rho_t}{M} P_{ij}(1 - P_{ij}) + o(1).
\end{aligned}
$$

Since $\widehat{P}_{ij} = \widehat{X}_i^\top \widehat{X}_j$ is asymptotically unbiased for P_{ij}, when n is large enough, we have

$$\mathbb{E}[(\widehat{P}_{ij} - P_{ij})^2] = \mathrm{Var}(\widehat{P}_{ij}) \approx \frac{1/\rho_s + 1/\rho_t}{MN} P_{ij}(1 - P_{ij}) + o(1).$$

$\square$

The proof for Theorem 4.2 is now a simple application of the above lemmas to the ratio of the mean squared errors for $\bar{A}$ and $\widehat{P}$.